Specific Emitter Identification Using Convolutional Neural Network-Based IQ Imbalance Estimators

LAUREN J. WONG[ID], WILLIAM CHRISTOPHER HEADLEY, AND ALAN J. MICHAELS
Center for National Security and Technology, Virginia Polytechnic Institute and State University, Blacksburg, VA 24060, USA
Corresponding author: Lauren J. Wong (ljwong@vt.edu)

ABSTRACT Specific Emitter Identification is the association of a received signal to a unique emitter, and is made possible by the naturally occurring and unintentional characteristics an emitter imparts onto each transmission, known as its radio frequency fingerprint. This paper presents an approach for identifying emitters using convolutional neural networks to estimate the inphase/quadrature (IQ) imbalance parameters of each emitter, using only the received raw IQ data as input. Because an emitter's IQ imbalance parameters will not change as it changes modulation schemes, the proposed approach has the ability to track emitters, even as they change the modulation scheme. The performance of the developed approach is evaluated using simulated quadrature amplitude modulation and phase-shift keying signals, and the impact of signal-to-noise ratio, imbalance value, and modulation scheme are considered. Furthermore, the developed approach is shown to outperform a comparable feature-based approach, while making fewer assumptions and using fewer data per decision.

INDEX TERMS Specific Emitter Identification (ESI), convolutional neural networks, IQ imbalance, estimation.

I. INTRODUCTION

Specific Emitter Identification (SEI) is the act of correlating an emitter with a received signal, using a database of radio frequency (RF) features. SEI algorithms are often used in military settings for emitter tracking [1], and have also become a powerful tool for use in cognitive radio applications to enforce Dynamic Spectrum Access (DSA) rules [2].

Current state-of-the-art SEI systems rely on the measurement of pre-determined and expert-defined signal features, which are then clustered by emitter for identification [1]. However, extracting expert features often requires considerable pre-processing of the raw signal data, such as synchronization, carrier tracking, demodulation, and signal-to-noise ratio (SNR) estimation, in addition to the computational cost of measuring or estimating the expert features. Further, these pre-determined features are often only accurate over a narrow range of parameters and require accurate and consistent measurement or estimation, in order to ensure quality SEI performance.

Features often used in traditional SEI algorithms are either taken from the transient or the steady-state portions of the received signal. When using features extracted from the transient signal, SEI performance relies heavily on the accuracy

The associate editor coordinating the review of this manuscript and approving it for publication was Yin Zhang.

and consistency of the transient detection and removal process, as this directly affects the quality of the features [3]. Though using features extracted from the steady-state portion of the received signal are generally more practical, expert features used to describe the steady-state signal often have their own limitations. For example, wavelet-based techniques are heavily impacted by the choice of wavelet function [4]. Further, preamble-based techniques fail when the received signal does not have a pre-defined preamble [3], and techniques analyzing the cyclostationary features of a signal are often inconsistent in the presence of frequency or phase uncertainties [5].

While neural networks have been used to perform the classification stage of SEI algorithms found in the literature, taking in pre-defined features as input [6], this work investigates the ability to perform emitter identification using neural networks to perform the feature extraction/estimation stage. More specifically, this work builds off of prior work in which an approach was developed using Convolutional Neural Networks (CNNs) to extract an expert feature, transmitter IQ imbalance [7]. Using the developed CNN IQ imbalance estimators described in Section III, an approach is presented in Section IV to identify emitters across numerous modulation schemes. Either the ability to determine the modulation class of the received signal, or that the modulation class of the received signal is known *a priori*, is assumed. However,
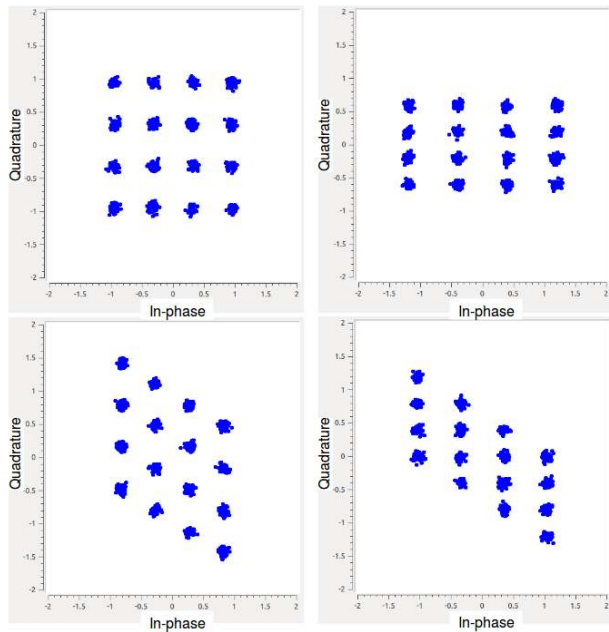
FIGURE 1. The result of transmitter IQ imbalance applied to the in-phase component of a 16QAM signal in the constellation diagram, SNR = 20dB. Top Left: no imbalances. Top Right: phase imbalance = 30°, gain imbalance = 0. Bottom Left: phase imbalance = 0, gain imbalance = 0.9. Bottom Right: phase imbalance = 30°, gain imbalance = 0.9.

under no circumstances is it assumed that the CNN input is adjusted for synchronization, carrier-tracking, SNR estimation, or demodulation. Performance analysis of the developed SEI approach is also given in Section IV, and shows the ability to identify emitters by their gain imbalance only with higher accuracy than a comparable feature-based approach.

II. TRANSMITTER IQ IMBALANCE
A. CAUSES AND IMPLICATIONS
Transmitter-induced, frequency-independent IQ imbalance is caused by non-idealities in the local oscillators, mixers, passives, and differential pair wiring of the transmitter which cause the in-phase and quadrature components of the modulator to be non-orthogonal. As a result, the real and imaginary components of the complex signal interfere with each other, which can increase the bit error rate of the communications system, if not properly accounted for. However, this hardware impairment can also be used to identify emitters, as emitters with differing levels of IQ imbalance will alter transmissions with different intensities.

The result of IQ imbalance in the real component of a 16QAM signal is shown in Fig. 1 in the constellation diagram and with exaggerated imbalance values for clarity. A phase imbalance, shown in the lower left constellation, results in the rotation of the real component of the symbols. Meanwhile a gain imbalance, shown in the upper right constellation, results in the stretching or contracting of the real component of the symbols.

In many systems, demodulation of the received signal may be impractical or impossible, such as in blind systems where
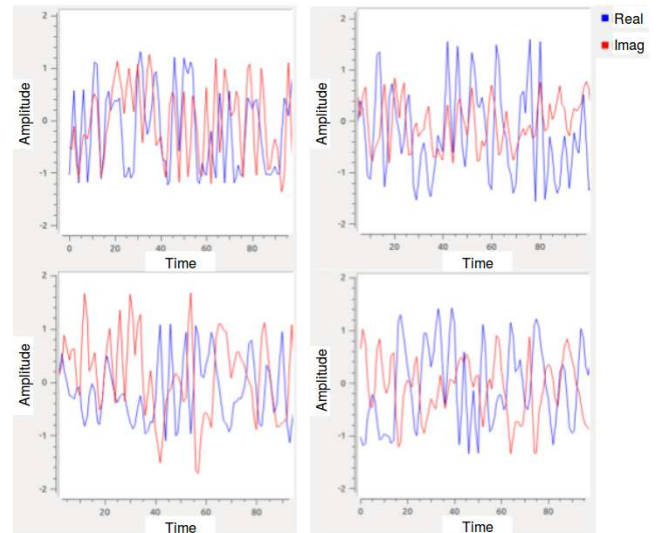

FIGURE 2. The result of transmitter IQ imbalance applied to the in-phase component of a 16QAM signal in the time domain, SNR = 20dB. Top Left: no imbalances. Top Right: phase imbalance = 30°, gain imbalance = 0. Bottom Left: phase imbalance = 0, gain imbalance = 0.9. Bottom Right: phase imbalance = 30°, gain imbalance = 0.9.

synchronization cannot be assumed. Therefore, the proposed approach uses only the raw received signal as input. This eliminates the need for demodulation which is required in many traditional SEI techniques [8].

The result of IQ imbalance on the real component of a 16QAM signal is shown in the time domain in Fig. 2 with the same imbalance values used in Fig. 1. In a transmitter with a phase imbalance, the phasor of the signal will be shifted, and in a transmitter with a gain imbalance, the amplitude of the signal will increase or decrease. While phase imbalances are more difficult to detect visually in the time domain, using the proposed approach developed in [7] and described in III, CNNs are capable of learning features which enable them to estimate both gain and phase imbalances, given enough input samples and reasonable SNR values.

B. SIGNAL MODEL
For simplicity, this work assumes only frequency-independent IQ imbalance, as is often assumed in existing literature [9]. Although most modern communications systems are affected by frequency-dependent IQ imbalance, frequency-independent IQ imbalance is a valid approximation for imbalanced narrowband systems and imbalance due to the analog components of emitters [9], [10]. Without loss of generality, all imbalances are modeled on the in-phase component of the modulated signal before transmission through an additive white Gaussian noise (AWGN) channel [11], as follows:

Consider the baseband signal

$$x(t) = x_i(t) + jx_q(t), \quad (1)$$

where $x_i(t)$ and $x_q(t)$ are real-valued time-varying baseband signals. An IQ modulator with IQ imbalance modulates this

baseband signal to its bandpass equivalent through

$$x(t) = (1 + \alpha)\cos(2\pi f_0 t + \theta)x_i(t) - j\sin(2\pi f_0 t)x_q(t), \quad (2)$$

where f_0 is the carrier frequency. In II-B, α is the transmitter's gain imbalance and θ is the transmitter's phase imbalance, such that an ideal transmitter, with no IQ imbalance, has $\alpha = 0$ and $\theta = 0°$. Then, the received signal, after transmission through an AWGN channel, is given by

$$y(t) = \mathbb{R}\left\{ \sum_{k=-\infty}^{\infty} (1 + \alpha)\cos(2\pi f_0 t + \theta)x_{k_i}(t) \right.$$
$$\left. - j\sin(2\pi f_0 t)x_{k_q}(t) \right\} + n(t) \quad (3)$$

where $n(t)$ is a zero-mean white Gaussian noise process [12], [13].

C. DATASET GENERATION

Using the signal model described above, all data used in the following simulation results were generated using the *gr-signal_exciter* module in GNURadio [14]. Though IQ imbalance parameters for real systems are not easily found, prior works in IQ imbalance estimation and compensation use test values ranging from 0.02 to 0.82 for absolute gain imbalance and from 2° to 11.42° for phase imbalance, with most works used test values on the orders of 0.05 and 5° for gain and phase imbalance respectively [8], [11], [13], [15]–[18]. Therefore, QAM signals of orders 8, 16, 32, and 64 and PSK signals of orders 2, 4, 8, and 16 were simulated with linear gain imbalances between $[-0.9, 0.9]$, uniformly distributed, and phase imbalances between $[-10°, 10°]$, uniformly distributed, in order to incorporate all possible offset values one might encounter in a real system. The effects of an imperfect signal detection stage were simulated also by applying frequency offsets between $[-0.1, 0.1]$ times the sample rate, uniformly distributed, and by sampling the simulated signal between $[1.2, 4]$ times Nyquist, uniformly distributed [19]. Then a root-raised cosine filter with a roll-off factor of 0.35 was applied to the sampled signal, and the signal was normalized to an average symbol power of 1dB. Finally, white Gaussian noise was added such that all signals had SNRs between $[0dB, 25dB]$, uniformly distributed.

III. CNN IQ IMBALANCE ESTIMATORS

In this section, the prior work [7] using CNNs to estimate IQ imbalance is described and expanded upon to include testing using PSK signals, as well as QAM signals, to show the designed architecture is modulation agnostic.

A. MODEL DESIGN, TRAINING, AND EVALUATION

The network architecture designed for the approach is shown in Fig. 3. The network contains two two-dimensional convolutional layers and four dense fully-connected layers, where the convolutional layers are designed to extract relevant features from the input signal and the fully-connected layers are designed to estimate the IQ imbalance on the signal, using
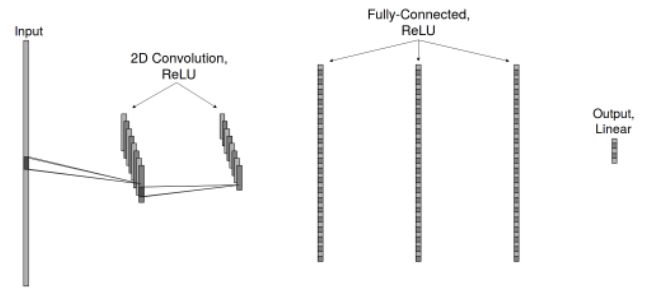

FIGURE 3. The CNN architecture designed for estimation of transmitter IQ imbalance.

the extracted features [20]. Though models were trained and evaluated using input sizes of 512, 1024, and 2048 raw IQ samples, in order to investigate the trade-offs between input-size and performance, the final models and those used in the SEI approach, use an input-size of 1024 samples, as this proved to be a good balance point between performance and network training and execution time. The Rectified Linear Unit (ReLU) activation function is used in every layer, except for the output layer which uses a linear activation function. Because the ReLU activation function zeroes out all negative values, the use of a linear activation function in the output layer allows the network to estimate negative gain and phase imbalance values. Stochastic gradient descent, with an RMSProp optimizer and a mean squared error loss function, was used to train the networks [21].

Two separate networks are trained to estimate gain imbalance and phase imbalance, allowing each network to be optimized for estimating gain and phase imbalance respectively. Both networks share the same architecture, but have different parameters and hyper-parameters and are not dependent. Therefore, they may be trained and run in parallel, or only one may be used, as is the case in the SEI approach presented in Section IV. An iterative script was use to select the best performing models after many iterations using different training parameters.

Separate networks are also trained to estimate IQ imbalance for the different modulation types simulated (QAM and PSK). However, results in Section III-B will show that the performance of these networks is comparable, indicating that the designed network architecture is modulation agnostic. It also should be noted that though the networks have been trained per modulation type, they are generalizing over modulation order (i.e. the networks trained to estimate IQ imbalance for QAM can estimate gain and phase imbalances for QAM signals of orders 8, 16, 32, and 64).

The normalized mean squared error (NMSE) was used to evaluate network performance [22]. Each network trained with a database containing 2000000 sets of labeled samples. Meanwhile, the validation and testing databases each contained 10000 sets of labeled samples. To further evaluate the performance of the estimators, evaluation sets were constructed containing 180000 and 200000 sets of samples for the gain imbalance estimator and the phase imbalance
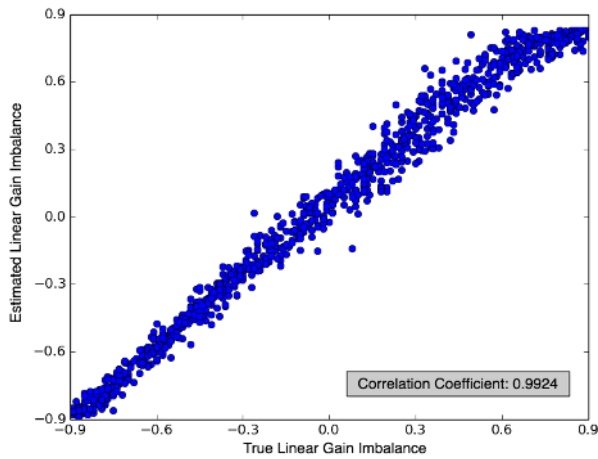
FIGURE 4. The true linear gain imbalance value versus the linear gain imbalance value estimated by the 1024-input CNN gain imbalance estimators with QAM input signals at 10dB SNR.
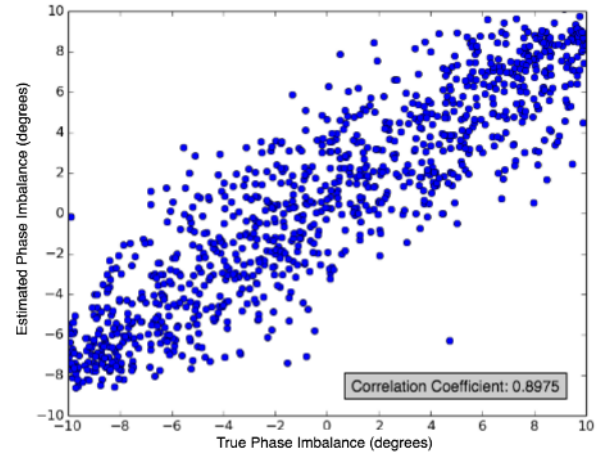

FIGURE 6. The true phase imbalance value versus the phase imbalance value estimated by the 1024-input CNN phase imbalance estimators with QAM input signals at 10dB SNR.
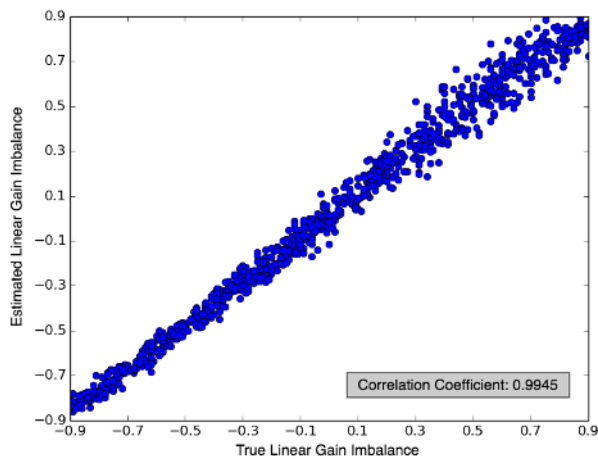

FIGURE 5. The true linear gain imbalance value versus the linear gain imbalance value estimated by the 1024-input CNN gain imbalance estimators with PSK input signals at 10dB SNR.
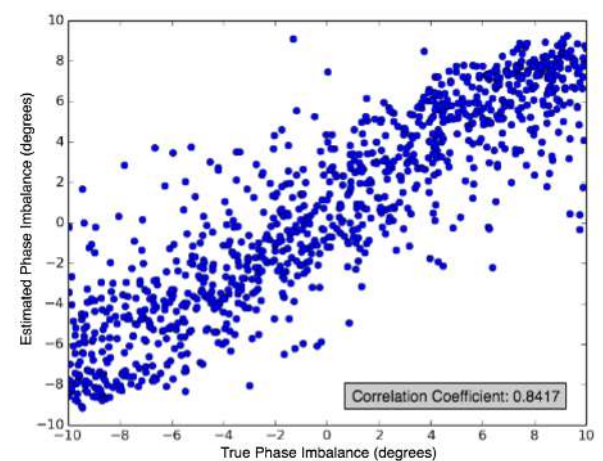

FIGURE 7. The true phase imbalance value versus the phase imbalance value estimated by the 1024-input CNN phase imbalance estimators with PSK input signals at 10dB SNR.

estimators respectively, such that 1000 sets of samples were generated at evenly spaced intervals of $\Delta\alpha = \pm 0.01$ and $\Delta\theta = \pm 0.1°$ within the training range.

B. SIMULATION RESULTS AND DISCUSSION

The initial results shown in Fig. 4-7 show the ability to estimate gain and phase imbalances, using the designed CNN architecture. However, the stronger linear correlations in Fig. 4 and 5 than in Fig. 6 and 7 indicate that phase imbalance is more difficult to estimate than gain imbalance. More input samples would likely produce better phase imbalance estimation results, providing more data to learn from. Similarly, a more sophisticated network architecture may also produce better phase imbalance estimation results.

The bias of the CNN IQ imbalance estimators was examined by taking the cumulative average of the CNN outputs for 1000 sets of samples with the same offset value. The estimator is called *unbiased* if the cumulative moving

average converges to the true offset value [23]. The bias and sample variance of the CNN IQ imbalance estimators is shown in Fig. 8-11, and shows the gain imbalance estimators have low bias and sample variance across all values within the training range (−0.9, 0.9). However, the bias of the gain imbalance estimators is slightly higher at positive offset values.

The results in Fig. 8-11 also show that phase imbalance estimators are significantly more biased than the gain offset estimators and have much higher sample variance compared to the gain imbalance estimators. This further indicates that phase imbalance is more challenging to estimate using the designed network architecture, at 10dB SNR. The bias of the phase imbalance estimators is lowest when the true offset value is near zero and increases as the magnitude of the true offset value increases. Meanwhile, the sample variance of the phase imbalance estimator outputs shows an inverse trend, further emphasizing the inaccuracy of the phase imbalance estimators.
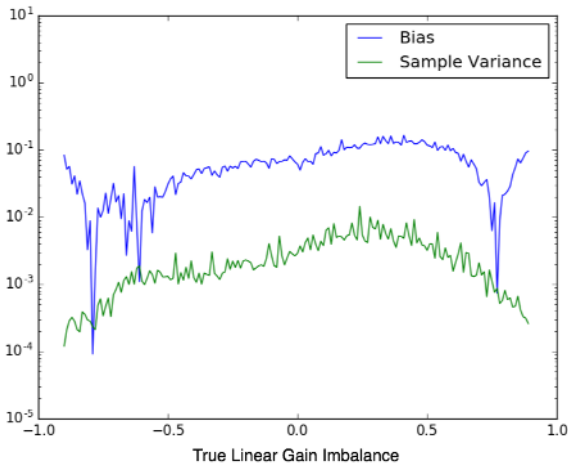
FIGURE 8. The bias and sample variance versus the true linear gain imbalance value for the 1024-input CNN gain imbalance estimator and QAM input signals simulated at 10dB SNR.
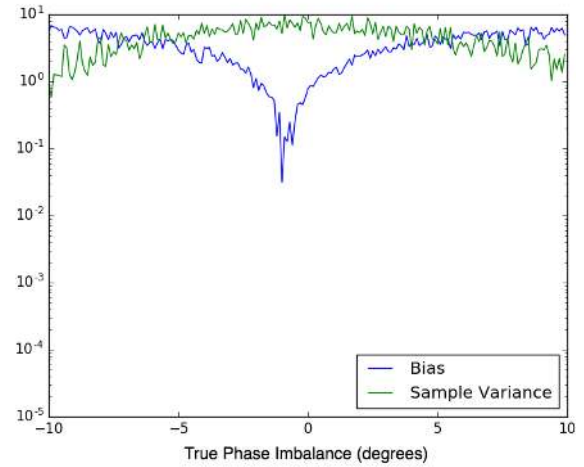

FIGURE 9. The bias and sample variance versus the true linear gain imbalance value for the 1024-input CNN gain imbalance estimator and PSK input signals simulated at 10dB SNR.

FIGURE 10. The bias and sample variance versus the true phase imbalance value for the 1024-input CNN phase imbalance estimator and QAM input signals simulated at 10dB SNR.
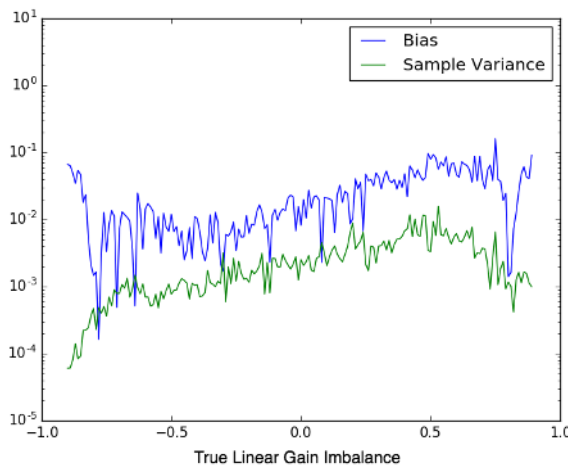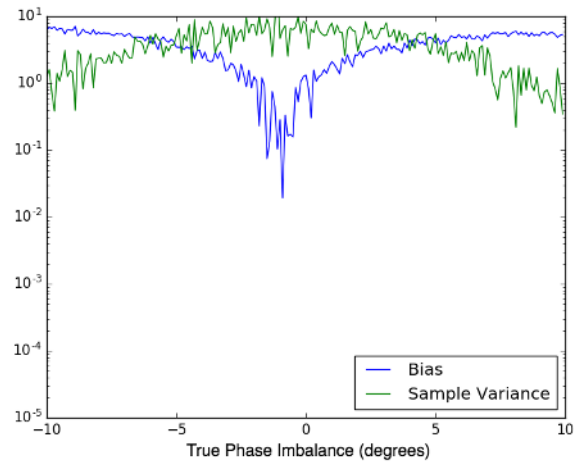

FIGURE 11. The bias and sample variance versus the true phase imbalance value for the 1024-input CNN phase imbalance estimator and PSK input signals simulated at 10dB SNR.

The performance of the CNN IQ imbalance estimators across various SNRs is shown in Fig. 12-15. More specifically, results show that as SNR increases, the Linear Gain Imbalance Estimation Error (the difference between the true and estimated imbalances) decreases, as expected. Additionally, as SNR increases, the standard deviation of the estimation error decreases with diminishing returns after 10dB. Meanwhile, the mean error remains constant near zero.

Fig. 16-19 show the effect of SNR and modulation scheme on the performance of the CNN IQ imbalance estimators using the average bias and sample variance of the estimator output. Consistent with the results shown in Fig. 12-15, Fig. 16-19 show that as SNR of the input signal increases, the average bias and sample variance of the estimator outputs decreases. Further, the CNN IQ imbalance estimators trained on PSK signals outperformed those trained on QAM signals, producing outputs with lower average bias and sample variance, especially when estimating gain imbalance. This is likely because QAM signals are both amplitude and phase

modulated, while PSK signals are only phase modulated, making gain imbalances harder to detect in QAM signals when only observing 1024 samples.

IV. TRANSMITTER GAIN IMBALANCE ESTIMATION FOR SEI

Three main steps are required to perform emitter identification using the CNN gain imbalance estimators, shown in Fig. 20: modulation classification, gain imbalance estimation, and decision making. The result is a decision tree-like structure in which the output of each step informs the next action, as described below.

Together, the results shown in the previous section indicated that the developed CNN IQ imbalance estimation architecture performs similarly when trained on PSK signals and when trained on QAM signals. As a result, the proposed SEI approach can be used when receiving signals with different modulation types. However, because the gain imbalance estimators are trained to be modulation-specific,
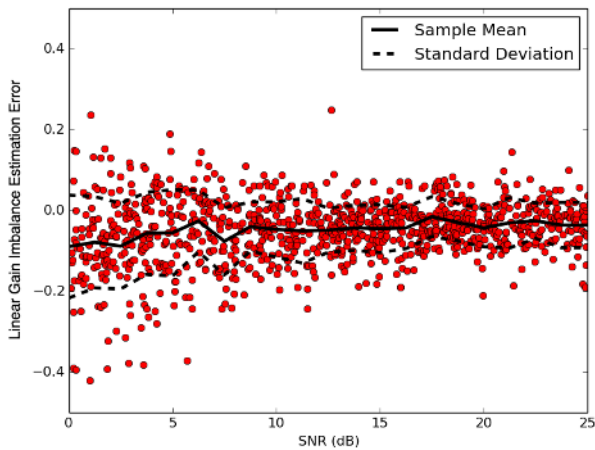
FIGURE 12. The linear gain imbalance estimation errors for signals simulated with SNRs between 0dB and 25dB. True linear gain imbalances vary uniformly between [−0.9, 0.9].

FIGURE 13. The linear gain imbalance estimation errors for signals simulated with SNRs between 0dB and 25dB. True linear gain imbalances vary uniformly between [−0.9, 0.9].

FIGURE 14. The phase imbalance estimation errors for signals simulated with SNRs between 0dB and 25dB. True phase imbalances vary uniformly between [−10°, 10°].
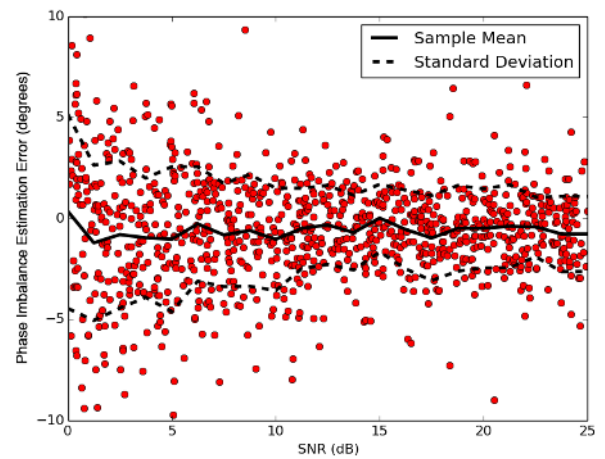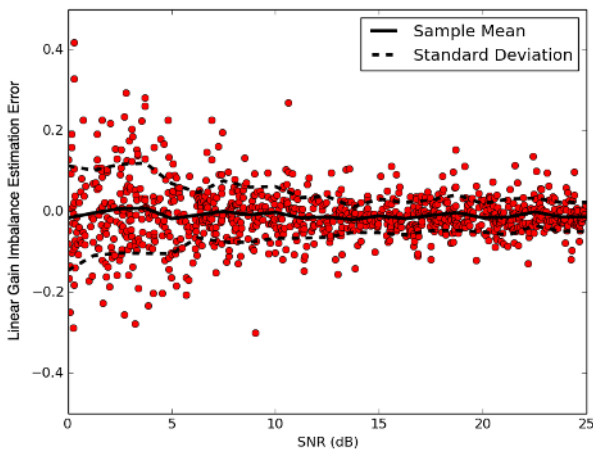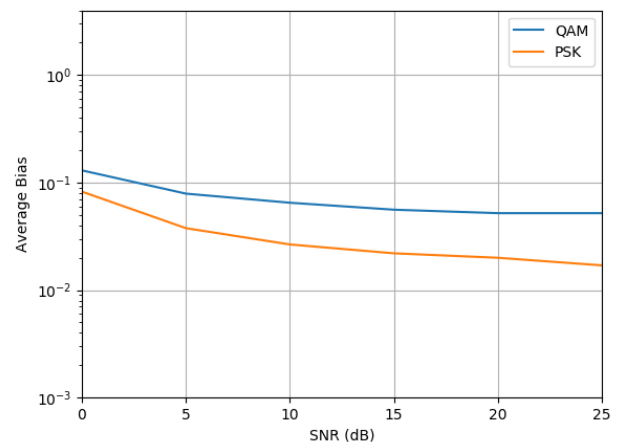

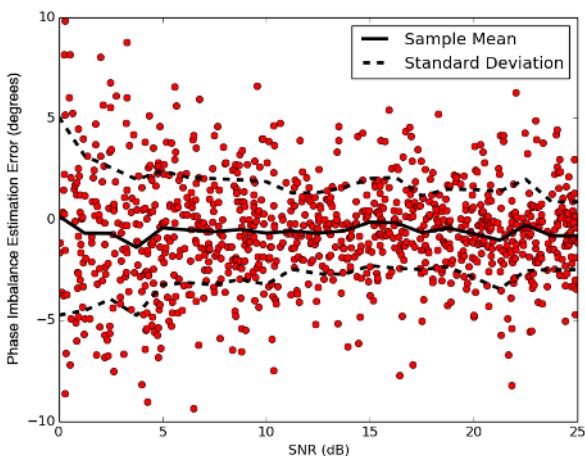**FIGURE 15.** The phase imbalance estimation errors for signals simulated with SNRs between 0dB and 25dB. True phase imbalances vary uniformly between [−10°, 10°].

FIGURE 16. The average bias versus SNR for the CNN gain imbalance estimators with input sizes of 512 samples, 1024 samples, and 2048 samples.

a modulation classification step is required in order to appropriately estimate the gain offset of each signal. It is important to note that while any modulation classifier may be used, a key advantage of the developed approach over traditional approaches is the use of only the raw IQ as input. In order to retain this advantage, the modulation classifier should also only use raw IQ as input. An example of such a classifier can be found in [19].

The output of the modulation classifier determines which modulation-specific CNN gain imbalance estimator is used in step two. The point estimate produced by the CNN gain imbalance estimator in step two is then used to determine the identity of the transmitter in step three using modulation-specific decision makers. These decision makers are composed of Gaussian probability density functions (*pdf*s), which have been fitted to the output of each CNN gain imbalance estimator, with Bayes optimal decision boundaries, as described below.

A. GAUSSIAN CURVE FIT TO CNN OUTPUT HISTOGRAMS
Using the evaluation sets described in Section III-A, histograms can be produced for the CNN estimator outputs at
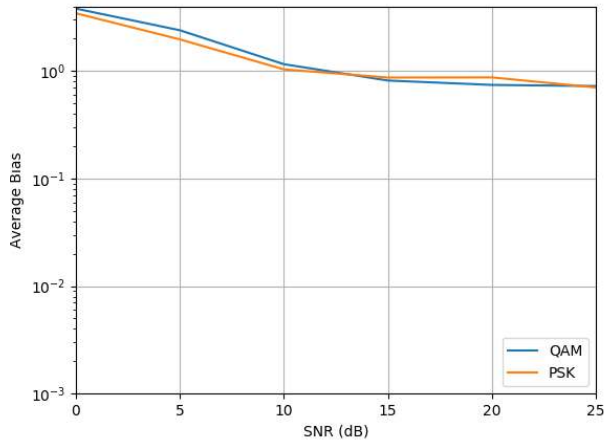
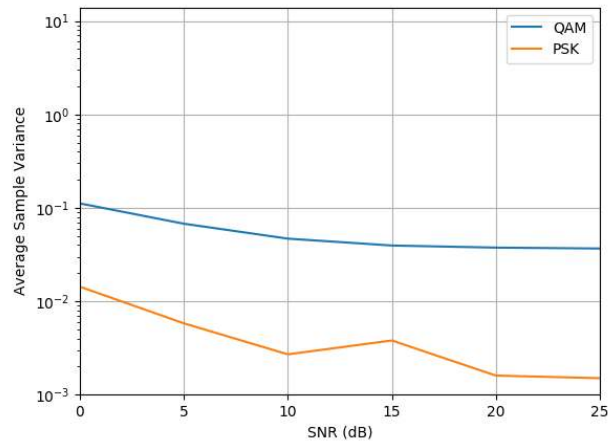**FIGURE 17.** The average bias versus SNR for the CNN phase imbalance estimators.

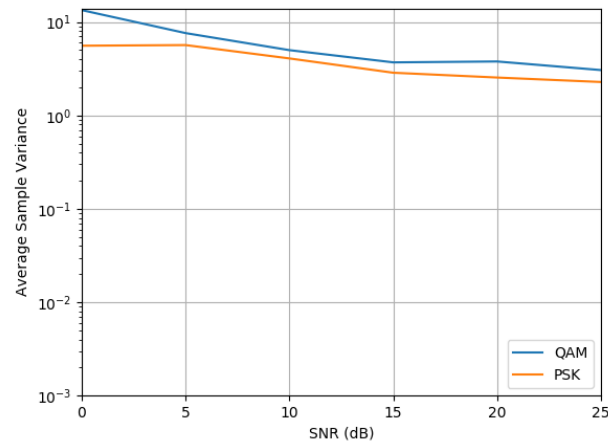**FIGURE 18.** The sample variance of the histograms for the CNN gain imbalance estimators as a function of SNR.

FIGURE 19. The sample variance of the histograms for the CNN phase imbalance estimators as a function of SNR.

FIGURE 20. The designed emitter identification approach using CNN IQ imbalance estimators.

FIGURE 21. The fitted Gaussian curve for the 1024 input CNN gain imbalance estimator output histogram with QAM input signals at 10dB SNR (Linear gain imbalance = 0.30).

p-value produced by the χ^2 test for both the QAM and PSK gain imbalance estimators, over all offset values. Because these values all exceed 0.5, a commonly chosen significance level in the literature [24], [25], the Gaussian distribution can be called an appropriate fit for the CNN gain imbalance estimator outputs.

B. BAYESIAN DECISION BOUNDARIES

After modulation classification and gain offset estimation, step three uses Bayesian decision boundaries between the fitted Gaussian *pdfs* to determine the identity of the emitter. Given two offset values, i and j, and fitted *pdf*s, $p(x|i)$ and $p(x|j)$, these decision boundaries are calculated as follows [26]. The following calculations assume that any given

evenly spaced intervals of 0.01 within the training interval, $[-0.9, 0.9]$. As mentioned above, Gaussian *pdf*s were fitted to these histograms (Fig.s 21 and 22), and the goodness of fit was tested using the Chi-Squared Goodness of Fit (GoF) test, as described in [7] and [24]. Table 1 shows the average
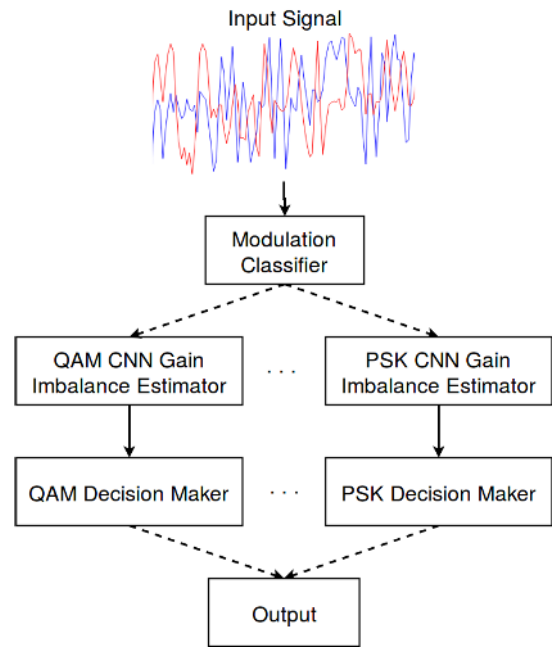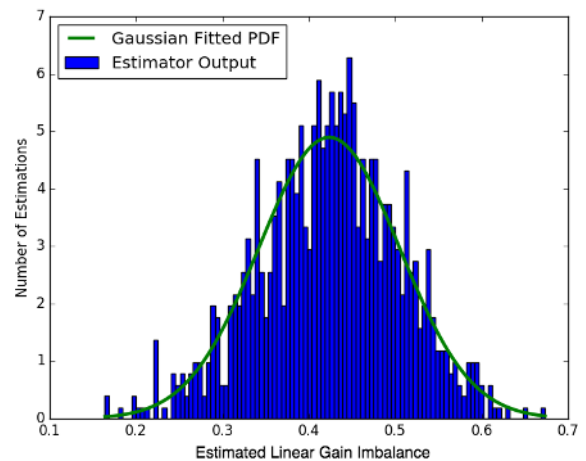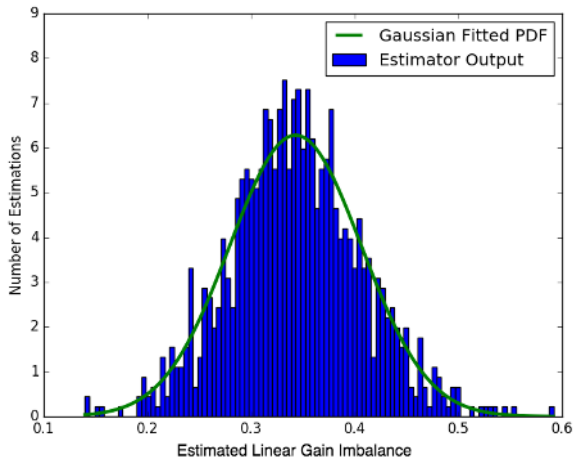
FIGURE 22. The fitted Gaussian curve for the 1024 input CNN gain imbalance estimator output histogram with PSK input signals at 10dB SNR (Linear gain imbalance = 0.30).

TABLE 1. The average *p*-values produced by the χ^2 GoF test.

	QAM	PSK
0dB	0.519	0.717
5dB	0.644	0.565
10dB	0.707	0.710
15dB	0.659	0.600
20dB	0.591	0.558
25dB	0.618	0.525

emitter is equally likely to have any gain imbalance value, but are not specific to the Gaussian *pdf* and can therefore be used for any curve fit.

Letting x be the received signal data,

Decide i if $P(i|x) > P(j|x)$; otherwise decide j.

Using Bayes Rule, this decision rule can be expressed in terms of the fitted *pdf*s ($p(x|i)$, $p(x|j)$) and the probability of the emitter have a given gain imbalance value ($P(i)$, $P(j)$):

Decide i if $p(x|i)P(i) > p(x|j)P(j)$; otherwise decide j.

Finally, assuming each gain imbalance value is equally likely to occur (i.e. $P(i) = P(j)$), the final decision rule is

Decide i if $p(x|i) > p(x|j)$; otherwise decide j,

making the decision boundary the intersection point(s) of the two fitted *pdf*s $p(x|i)$ and $p(x|j)$ for gain imbalance values i and j. More specifically, the decision boundary is $d = p(x|i) = p(x|j)$, as shown in Fig. 23.

C. DECISION MAKING

Given a decision boundary, d, calculated between the two *pdf*s for gain imbalance values i and j and a received signal, a decision can be made about emitter identity as follows:

After modulation classification, the received signal is fed to the appropriate gain imbalance estimator, producing a point estimate, x_i, of the gain imbalance of the emitter which sent
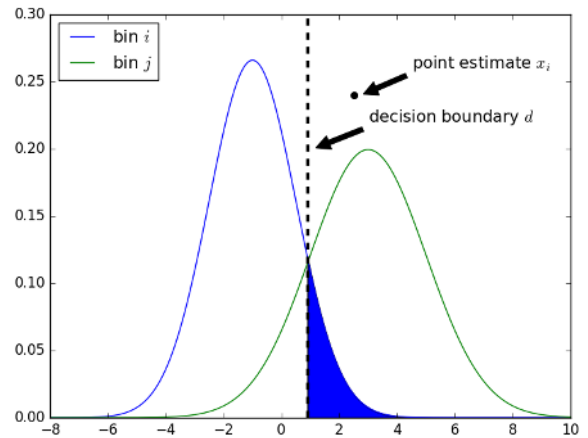

FIGURE 23. An example decision scenario.

the signal. Without loss of generality, let the mean of $p(x|i)$ be less than the mean of $p(x|j)$, as shown in the example decision scenario in in Fig. 23. If the point estimate falls on the left side of the decision boundary, it is decided the transmitted signal came from an emitter with gain imbalance value i. Otherwise, it is decided the transmitted signal came from an emitter with gain imbalance value j.

In the case that the emitters in the system are known, the *pdf*s of the known gain imbalance values can be selected and the decision boundaries between these *pdf*s calculated. Decisions on point estimates are then made as described above. While this method has use cases for Dynamic Spectrum Access and cooperative scenarios [27], the ability to perform SEI in non-cooperative and blind scenarios is a primary motivator of this work. In this case, when the emitters in the system are not known, the approach may still be used. However, because the *pdf*s of the known gain imbalance values cannot be selected, it is only possible to bin the emitters by their gain imbalance value by selecting and calculating the decision boundaries between evenly spaced *pdf*s. For simplicity, the results shown in Section IV-F will consider only this second case.

D. THE PROBABILITY OF MIS-IDENTIFYING EMITTERS

Given two fitted *pdf*s, $p(x|i)$ and $p(x|j)$, and the optimal decision boundary, d, between the *pdf*s, the probability of incorrectly identifying an emitter is given by

$$\int_d^\infty p(x|i)dx.$$

As an example, consider the scenario in Fig. 23, where a point estimate, x_i, is produced from a set of samples received from an emitter belonging to gain imbalance bin i. Again, without loss of generality, let the mean of $p(x|i)$ be less than the mean of $p(x|j)$. A correct classification occurs when the estimate from the CNN, x_i, is less than the decision boundary d. Therefore, an incorrect classification occurs when $x_i > d$.
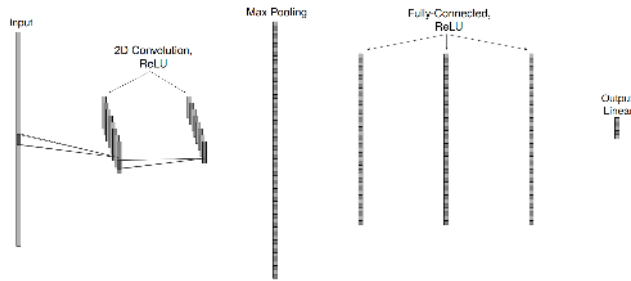
FIGURE 24. The CNN architecture designed for estimation of transmitter gain imbalance to perform SEI.

E. MODEL DESIGN, TRAINING, AND EVALUATION

The CNN gain imbalance estimation model used in the developed approach is the same as described in Section III-A, modified with one max-pooling layer, with size $= 2$, between the convolutional layers and the dense layers, as shown in Fig. 24.

When determining which networks performed best, the NMSE was no longer a helpful evaluation metric, as a network with a low average NMSE could produce histograms with larger variance than networks with a higher average NMSE. Therefore, to evaluate the performance of the trained networks, the evaluation sets previously described in Section III-A were used. For a given trained network, *pdf*s were fitted for each of the gain imbalance values, and the minimum gain imbalance separation needed to obtain a probability of mis-identification of less than 5% was calculated. This minimum gain imbalance separation value was used to determine which networks were performing better than others.

F. SIMULATION RESULTS AND DISCUSSION

To fully analyze the performance of the designed SEI approach, the following sections investigate the effect of SNR, true gain imbalance value, and modulation scheme on the SEI decision, and compare the designed approach to a traditional feature-based approach. Further, the practicality of using the designed approach is discussed, considering the IQ imbalance values typically found in real systems and the assumptions typically made by traditional SEI systems.

1) IMPACT OF SNR ON SEI PERFORMANCE

Using the evaluation sets constructed for QAM and PSK, the minimum gain imbalance separations needed to obtain average probabilities of mis-identification of less 20%, 10%, and 5% across all gain imbalance values were calculated, as described in Section IV-D. The impact of SNR on the ability to identify emitters at these levels of accuracy is shown in Fig.s 25 and 26. At $0dB$, the estimators cannot be used to perform emitter identification to a 80% probability of correct identification. However, as the SNR increases, the minimum gain imbalance separation needed to obtain $< 5\%$, $< 10\%$, and $< 20\%$ probabilities of mis-identification decreases with diminishing returns at around $20dB$. Therefore, the lower the probability of mis-identification needed in
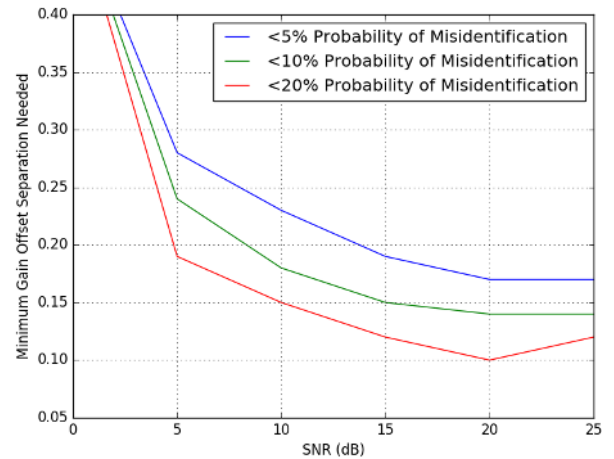

FIGURE 25. The SNR vs minimum gain imbalance separation needed to obtain < 5%, < 10%, and < 20% probability of mis-identification using the CNN gain imbalance estimator trained on QAM input signals.
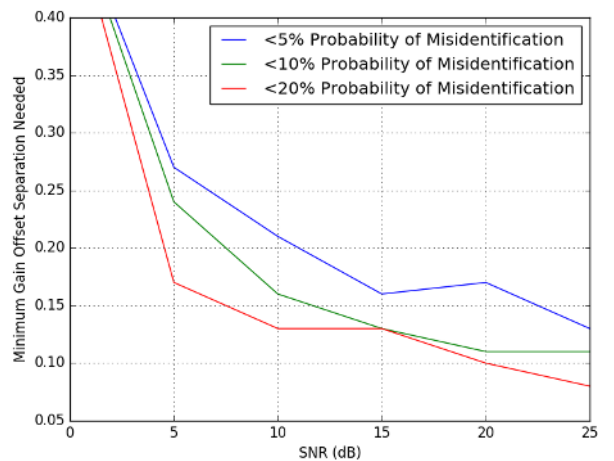

FIGURE 26. The SNR vs minimum gain imbalance separation needed to obtain < 5%, < 10%, and < 20% probability of mis-identification using the CNN gain imbalance estimator trained on PSK input signals.

a system, the higher the gain imbalance separation needed, as expected.

2) IMPACT OF GAIN IMBALANCE VALUE ON SEI ABILITY

In Section III-B and Fig. 8 and 9, it was shown that the sample variance of the gain imbalance estimators is slightly lower when the true offset value is at the limits of the training range (near -0.9 and 0.9). As a result, the variance of the fitted *pdf*s is lower when the true gain imbalance value is near the limits of the training range, in comparison to when the true gain imbalance value is near zero. Therefore, the probability of mis-identification is lower when the true gain imbalance value is near the limits of the training range.

3) IMPACT OF MODULATION SCHEME ON SEI PERFORMANCE

The ability to perform gain imbalance estimation on QAM and PSK signals using the designed CNN architecture was shown in Section III-B. Though the use of CNN estimators
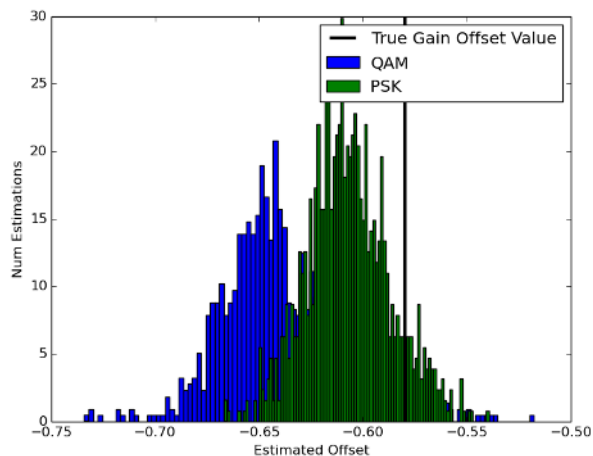
FIGURE 27. The histogram outputs for the PSK and QAM estimators both with true gain imbalance value of -0.58.

TABLE 2. The simulated IQ Imbalance parameters used for comparison to the approach proposed in [28].

	Emitter 1	Emitter 2	Emitter 3	Emitter 4	Emitter 5
α	0.1	0.13	0.15	0.17	0.19
θ	3°	3.3°	3.6°	3.9°	4.2°

for gain imbalance estimation on other signal types was not investigated, the comparable results of the CNN gain imbalance estimators trained for QAM and PSK showed that the designed network architecture described in Section III-A was not modulation specific. Investigation into the performance of the estimators on further modulation schemes is left for future work.

Fig. 27 shows the importance of having separate decision boundaries for each modulation class. Though the true gain imbalance value of the input signal to the estimators is the same, the output histograms produced by the modulation-specific CNN gain imbalance estimators are not. This yields different decision boundaries for each modulation class.

As discussed in Section III-B and shown in Figs. 18 and 19, the CNN gain imbalance estimator trained for PSK showed lower average sample variance than the CNN gain imbalance estimator trained for QAM. This resulted in fitted *pdf*s with lower variance for PSK than QAM. Therefore, in general, lower minimum gain imbalances are needed to identify emitters when transmitting PSK signals than are needed to identify emitters when transmitting QAM signals, as shown in Fig. 25 and 26. As a result, more emitters can be identified uniquely.

4) PRACTICAL CONSIDERATIONS
As previously mentioned, for both QAM and PSK, the lower the probability of mis-identification needed in a system, the higher the gain imbalance separation needed to achieve the needed level of accuracy. Therefore, in systems with a higher tolerance for mis-identification, more emitters can be uniquely identified, and in systems that require a low probability of mis-identification, fewer emitters can be uniquely identified. However, even in systems with a 20% tolerance for mis-identification and receiving signals exceeding 20*dB* SNR, the emitters need to have a linear gain imbalance separation of at least 0.15. While few publications indicate measured gain imbalance values for real systems, most prior works in IQ imbalance estimation and compensation use

test values on the order of 0.05 [8], [11], [13], [15]–[18], indicating the gain imbalance values necessary to obtain even 80% accuracy are not practical in real systems. Narrowing the range of gain imbalance values included in the training set would likely help combat this problem.

The training set was simulated with gain imbalances between [−0.9, 0.9], uniformly distributed, in order to incorporate any possible gain imbalance value the CNN estimator might encounter in a real system. However, training over such a large range has likely hindered the estimator's accuracy, as the network has had to learn to generalize over such a large range [19]. Given that an offset value of 0.9 is likely much larger than anything one might find in a real system, the training range could be narrowed to yield better results in estimator accuracy and therefore SEI ability.

5) COMPARISON TO A TRADITIONAL FEATURE-BASED APPROACH
In [28], an SEI approach was developed using IQ imbalance estimates and Support Vector Machines (SVMs). The IQ imbalance estimation algorithm proposed uses statistical methods to determine gain and phase imbalance using the received symbols. The approach also requires SNR estimation. They then plot gain versus phase imbalance in two dimensions and use SVMs to assign the received signal to an emitter.

In order to provide an accurate comparison of the approach proposed in [28], five QPSK emitters were simulated with gain and phase imbalance values given in Table 2, for SNRs between [5dB, 35dB] at intervals of 5dB, and with perfect synchronization, as in [28]. The developed CNN gain imbalance estimator was also retrained to accommodate these assumptions. More specifically, a CNN gain imbalance estimator was retrained using training, validation, and test sets with SNRs between [0dB, 35dB], gain imbalance values (α) between [0.0, 0.3], phase imbalance values (θ) between [0°, 5°], and no frequency or sample rate offsets, matching the assumptions in [28].

The results in Fig. 28 show the accuracy of the approach developed in this chapter to that proposed in [28], given one capture of 1024 raw IQ samples and given ten captures of 1024 raw IQ samples. When the approach developed in this chapter uses only one capture of 1024 raw IQ samples, the developed approach shows lower accuracies than the approach presented in [28] by as much as 15%. However, it is important to note the developed approach uses only estimates of gain imbalance, while the approach presented in [28] uses estimates of both gain and phase imbalance, providing more information about the emitter-of-interest. Phase imbal-
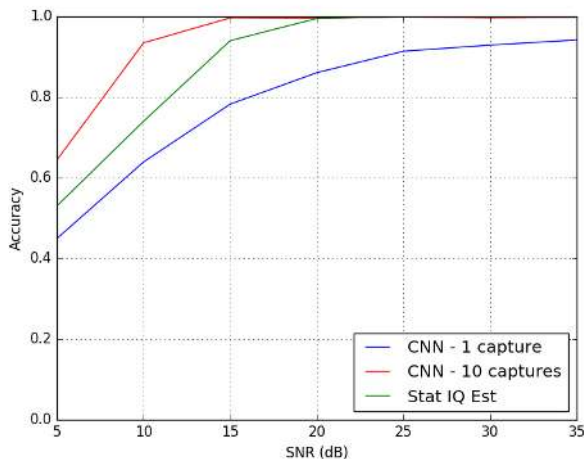
FIGURE 28. The accuracy of the developed SEI approach using CNN gain imbalance estimators compared to the accuracy of the approach proposed in [28], given one and ten captures of 1024 raw IQ samples.
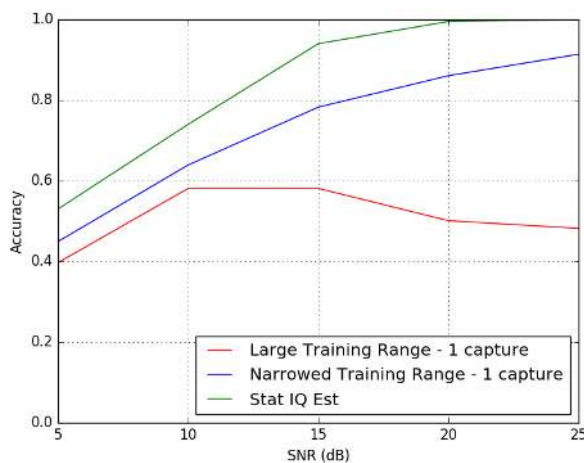

FIGURE 29. The accuracy of the developed SEI approach using the large training range described in Section II-C compared to the accuracy using the narrowed training range used to match the assumptions made in [28].

ance estimates could also be incorporated into the approach developed in this chapter, and would likely increase performance. The approach presented in [28] is also dependent upon an estimate of SNR and assumes perfect synchronization, whereas the approach developed in this chapter needs no external measurements or estimates and can compensate for an imperfect receiver. Additionally, the accuracy of the approach proposed in [28] is calculated given 1330 symbols, whereas the accuracy of the approach developed in this chapter is given for one capture of 1024 raw IQ samples. For the proposed approach, the outputs of multiple raw IQ captures can be aggregated to improve accuracy, as shown in Fig. 28. Therefore, given as few as ten captures of 1024 raw IQ samples, the accuracy of the approach developed in this chapter exceeds the performance of the approach proposed in [28], using less data and making far fewer assumptions.

It should also be noted that limiting the range of IQ imbalance parameters and assuming perfect synchronization has improved the performance of the developed approach,

as shown in Fig. 29. This confirms that training over smaller parameter ranges, more closely aligned with those one might find in a real system, can improve performance, and is consistent with the results and discussion in [19].

V. SUMMARY AND FUTURE WORK

This work expanded upon prior work showing the ability to estimate transmitter-induced and frequency-independent IQ imbalance using CNNs by showing the previously developed models to be modulation agnostic [7]. More specifically, performance analysis of the previously developed CNN IQ imbalance estimators showed the ability to estimate both gain and phase imbalances, when trained using QAM and PSK signals. Further, an approach was designed and evaluated using parallel, modulation-specific, gain imbalance estimators to identify emitters.

Results show that for both QAM and PSK modulation schemes, the performance of the proposed SEI increases as SNR increases, in the form of smaller gain imbalance separations needed to achieve lower probabilities of mis-identification. However, because the gain imbalance estimators trained for PSK slightly outperformed those trained for QAM, the proposed SEI approach performed better when the incoming signal was of a PSK modulation scheme. The approach was shown to need impractical gain imbalance separation values, even in high SNR scenarios, when the range of IQ imbalance parameters included in the training set is large, but performance improved significantly when this range was narrowed. Further, the accuracy of the approach was shown to exceed that of a traditional feature-based approach, given as few as ten captures of 1024 raw IQ samples.

To improve the proposed SEI approach, the range of gain imbalance values included in the training set can be narrowed, so that the network has to generalize less. This was shown when comparing the developed approach to the approach in [28]. The addition of more hardware impairments to the model, in order to further discriminate emitters, would also likely increase performance and is left for future work. Finally, this work could also be extended to further modulation schemes, different channel models, and to receiver IQ imbalance.

REFERENCES

[1] K. I. Talbot, P. R. Duley, and M. H. Hyatt, "Specific emitter identification and verification," *Tech. Rev.*, vol. 113, p. 113, 2003.

[2] J.-M. Park, J. H. Reed, A. A. Beex, T. C. Clancy, V. Kumar, and B. Bahrak, "Security and enforcement in spectrum sharing," *Proc. IEEE*, vol. 102, no. 3, pp. 270–281, Mar. 2014.

[3] G. Huang, Y. Yuan, X. Wang, and Z. Huang, "Specific emitter identification based on nonlinear dynamical characteristics," *Can. J. Electr. Comput. Eng.*, vol. 39, no. 1, pp. 34–41, winter 2016.

[4] C. Bertoncini, K. Rudd, B. Nousain, and M. Hinders, "Wavelet finger-printing of radio-frequency identification (RFID) tags," *IEEE Trans. Ind. Electron.*, vol. 59, no. 12, pp. 4843–4850, Dec. 2012.

[5] K. W. Kim, "Exploiting cyclostationarity for radio environmental awareness in cognitive radios," Ph.D. dissertation, Dept. Elect. Comput. Eng., Virginia Polytech. State Univ., Blacksburg, VA, USA, 2008.

[6] J. Matuszewski and K. Sikorska-Łukasiewicz, "Neural network application for emitter identification," in *Proc. 18th Int. Radar Symp. (IRS)*, Jun. 2017, pp. 1–8.

[7] L. J. Wong, W. C. Headley, and A. J. Michaels, "Estimation of transmitter I/Q imbalance using convolutional neural networks," in *Proc. IEEE 8th Annu. Comput. Commun. Workshop Conf. (CCWC)*, Jan. 2018, pp. 948–955.

[8] L. Angrisani, M. D'Arco, and M. Vadursi, "Clustering-based method for detecting and evaluating I/Q impairments in radio-frequency digital transmitters," *IEEE Trans. Instrum. Meas.*, vol. 56, no. 6, pp. 2139–2146, Dec. 2007.

[9] Y. Li, "Frequency independent IQ imbalance estimation and compensation," in *In-Phase and Quadrature Imbalance*. New York, NY, USA: Springer, 2014, pp. 29–47.

[10] D. L. N. S. Inti, "Time-varying frequency selective IQ imbalance estimation and compensation," M.S. thesis, Dept. Elect. Eng., Virginia Polytech. State Univ., Blacksburg, VA, USA, 2017.

[11] C. J. Hsu and W. H. Sheen, "Joint calibration of transmitter and receiver impairments in direct-conversion radio architecture," *IEEE Trans. Wireless Commun.*, vol. 11, no. 2, pp. 832–841, Feb. 2012.

[12] J. G. Proakis and M. Salehi, *Digital Communications*, 5th ed. New York, NY, USA: McGraw-Hill, 2008.

[13] C.-L. Liu, "Impacts of I/Q imbalance on QPSK-OFDM-QAM detection," *IEEE Trans. Consum. Electron.*, vol. 44, no. 3, pp. 984–989, Aug. 1998.

[14] Bill Clark. (Sep. 2016). *Efficient Waveform Spectrum Aggregation for Algorithm Verification and Validation*. [Online]. Available: https://gnuradio.org/grcon-2016/talks/

[15] F. E. Churchill, G. W. Ogar, and B. J. Thompson, "The correction of I and Q errors in a coherent processor," *IEEE Trans. Aerosp. Electron. Syst.*, vol. AES-17, no. 1, pp. 131–137, Jan. 1981.

[16] S. A. Bassam, S. Boumaiza, and F. M. Ghannouchi, "Block-wise estimation of and compensation for I/Q imbalance in direct-conversion transmitters," *IEEE Trans. Signal Process.*, vol. 57, no. 12, pp. 4970–4973, Dec. 2009.

[17] D. S. Hilborn, S. P. Stapleton, and J. K. Cavers, "An adaptive direct conversion transmitter," *IEEE Trans. Veh. Technol.*, vol. 43, no. 2, pp. 223–233, May 1994.

[18] S. Burglechner, G. Hueber, and A. Springer, "On the estimation and compensation of IQ impairments in direct conversion transmitters," in *Proc. Eur. Conf. Wireless Technol.*, Oct. 2008, pp. 69–72.

[19] S. C. Hauser, W. C. Headley, and A. J. Michaels, "Signal detection effects on deep neural networks utilizing raw IQ for modulation classification," in *Proc. IEEE Mil. Commun. Conf. (MILCOM)*, vol. 1, Oct. 2017, pp. 121–127.

[20] K. Jarrett, K. Kavukcuoglu, M. Ranzato, and Y. LeCun, "What is the best multi-stage architecture for object recognition?" in *Proc. IEEE 12th Int. Conf. Comput. Vis.*, Oct. 2009, pp. 2146–2153.

[21] G. Hinton, N. Srivastava, and K. Swersky, "Neural networks for machine learning lecture 6A overview of mini-batch gradient descent," Univ. Toronto, Toronto, ON, Canada, Tech. Rep., 2012.

[22] L. Patryla and D. Galeriua, "Statistical performances measures—Models comparison," Tech. Rep., 2011.

[23] G. W. Brown, "On small-sample estimation," *Ann. Math. Statist.*, vol. 18, no. 4, pp. 582–585, Dec. 1947.

[24] K. Pearson, *On the Criterion that a Given System of Deviations from the Probable in the Case of a Correlated System of Variables is Such that it Can be Reasonably Supposed to Have Arisen from Random Sampling*. New York, NY, USA: Springer, 1992, pp. 11–28.

[25] P. E. Greenwood and N. M. Stepanovic, *A Guide to Chi-Squared Testing*. Hoboken, NJ, USA: Wiley, 1996.

[26] R. O. Duda, P. E. Hart, and D. G. Stork, *Pattern Classification*, 2nd ed. Hoboken, NJ, USA: Wiley, 2000.

[27] M. Song, C. Xin, Y. Zhao, and X. Cheng, "Dynamic spectrum access: From cognitive radio to network radio," *IEEE Wireless Commun.*, vol. 19, no. 1, pp. 23–29, Feb. 2012.

[28] F. Zhuo, Y. Huang, and J. Chen, "Radio frequency fingerprint extraction of radio emitter based on I/Q imbalance," *Procedia Comput. Sci.*, vol. 107, pp. 472–477, Jan. 2017.

LAUREN J. WONG received an M.S. degree in electrical engineering from Virginia Tech (VT), and the B.A. degree in computer science and mathematics from Oberlin College. She is currently pursuing a Ph.D. degree in electrical engineering with VT, where she is also a Research Associate with the Virginia Tech Hume Center. Her research focuses in various aspects and applications of RFML.

WILLIAM CHRISTOPHER HEADLEY received B.S., M.S., and Ph.D. degrees in ECE from Virginia Tech, where he is currently a Research Assistant Professor with the Virginia Tech Hume Center. His current research interests deal with the intersection of digital signal processing, spectrum sensing, and machine learning.

ALAN J. MICHAELS received B.S., M.S., and Ph.D. degrees in ECE, B.S. and M.S. degrees in applied math, and an M.S. degree in operations research from Georgia Tech, and an MBA degree from Carnegie Mellon University. He serves as the Director of the Electronic Systems Research with the Virginia Tech Hume Center. Prior to joining VT, he spent a decade in industry, leading research efforts in secure communications, with a particular focus in chaotic sequence spread spectrum systems. He holds 40 U.S. patents.

● ● ●